J. SAWICKI*#, J. ŚWINIARSKI**, M. STEGLIŃSKI*, P. BYCZKOWSKA*

NUMERICAL ANALYSIS OF TWIST EXTRUSION PRESSING OF Al-Mg-Mn-Sc-Zr SCALMALLOY

Twist extrusion is a processing method involving the extrusion of a sample with a prismatic cross-section using a tool composed of four prismatic parts bisected by a screw component. A beneficial change in mechanical durability is one of the main factors enabling the use of highly durable Al-Mg-Mn-Sc-Zr alloys to construct functional components of non-stationary robots. As part of the present research, ANSYS® software was used to simulate a twist extrusion process. An analysis of a sample entering and passing through the entire twisting area was performed, up to the point of full twisting of the base of the sample. The stress conditions in the sample were analysed as it passed through the twisting area. The highest stress values (reaching up to 600 MPa) were detected at the tips of the sample face as the sample exited the twisting area. The lowest stress values, at around 170 MPa, were detected at the side edges of the sample.

Keywords: aluminium alloys; twist extrusion; numerical analyses, residual stresses

1. Introduction

Severe Plastic Deformation plastic processing methods have been known for a long time and are becoming more and more popular. SPD methods are primarily used for grain refinement [1-8], resulting in the transformation of the micrometric structure of materials into ultrafine-grained (grain size 500÷100 nm) or nanometric (grain size <100 nm) structure [9-12]. Most popular SPD processing methods include ECAP, HPT and TE

The use of this type of processing methods results in plastic deformations and generation of residual compression stresses in the upper layer of the processed component [13-19]. The distribution of stress values and their ranges within the processed material depend on the parameters of the SPD process. Obtaining the required alloy durability parameters requires a number of experiments in order to ascertain the best processing parameters. A numerical study of the methodology of construction and solution of process models utilising an intensive accumulation of SPD deformations is of key importance to ensuring control of technological processes. By using computer simulations, we can gain a deeper understanding of the physical processes that occur when a component is processed and their impact on the mechanical properties of the processed material. Analysis of these phenomena will enable choosing optimal parameters of the process and verifying its assumptions and remedying any errors already at the computer simulation stage, significantly shortening the time needed for implementation and reducing costs.

Two shear planes appear during the TE process – at the entry to and exit from the twisting area. The line of the shear plane is perpendicular to the axis of the sample. When passing through the twisting area, the material increases its surface by 70-80% and returns to its original size after exiting the twisting area [20]. The direction of the movement of the material remains the same throughout the process. Furthermore, the amount of wasted material is relatively low compared to other SPD techniques (e.g. ECAP) [21]

The section area and the dimensions of the component remain unchanged throughout the process, making it possible to repeat the process several times in order to accumulate stresses required to change the microstructure and mechanical properties of the sample [22].

In contrast to ECAP and HPT, one of the basic features of the TE process is the ability to generate two deformation planes within a single process iteration, as well as the ability to ensure continuity of the process. Neither of the above can be achieved in ECAP, where only a single deformation plane is generated, and HPT, where the process is non-continuous. Thanks to the above features, TE processing can potentially be used to improve the durability of aluminium alloys, provided, however, that the design and technological parameters of the alloy are selectively determined.

2. Material and methodology

An RSA-501 aluminium alloy, with the following composition: Al; Mg 5%; Mn 1.5%; Sc 0.8%; Zr 0.4% (a scalmalloy), was used in the research. The parameters of the material subjected to

* LODZ UNIVERSITY OF TECHNOLOGY, INSTITUTE OF MATERIALS SCIENCE AND ENGINEERING, 1/15 STEFANOWSKIEGO STR., 90-924 LODZ, POLAND
** LODZ UNIVERSITY OF TECHNOLOGY, DEPARTMENT OF STRENGTH OF MATERIALS, 1/15 STEFANOWSKIEGO STR., 90-924 LODZ, POLAND,
# Corresponding author: jacek.sawicki@p.lodz.pl

pressing were determined experimentally, in accordance with the requirements of standard EN ISO 6892-1, using an Instron universal static tensile testing machine equipped with a Zwick-Roell measurement system (Fig. 1), and entered into the numerical software. The model of the material used in MES calculations is described in the ANSYS® system as linearly elastic up to the yield limit, and as non-linear beyond that limit.
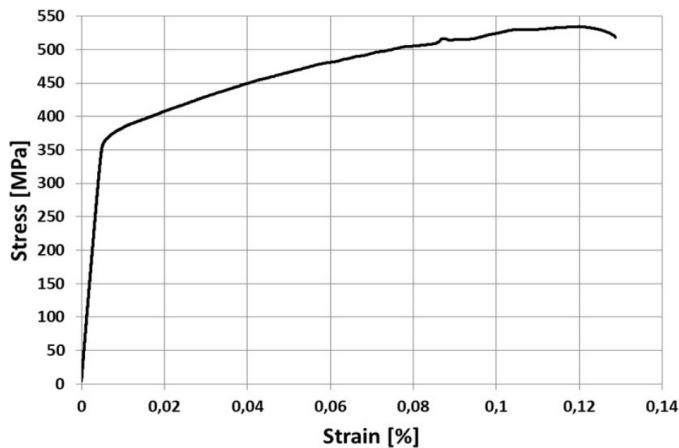

Fig. 1. Stress-strain curve for the RSA-501 aluminium alloy

After performing durability tests in order to determine the material parameters of the RSA-501 aluminium alloy, an additional series of tests was performed in respect of three different tensioning speeds, in order to analyse the behaviour of the sample depending on tensioning speed.

The samples were subjected to variable forces at a constant tensioning speed: 200 mm/min, 400 mm/min and 600 mm/min. Test results can be seen in Fig. 2.
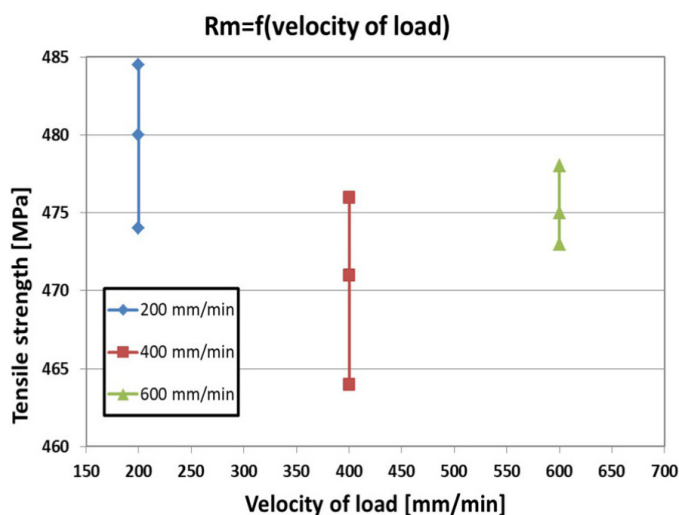

Fig. 2. Relationship between ultimate tensile stress and velocity of the load under tensile test

As can be seen, the highest yield limit and highest stresses were generated in samples tensioned with the lowest speed, although the differences between various tensioning speeds

were not significant. However, the above indicates that in order to generate the largest elongation of the material and highest tensioning values, the material should be tensioned at a relatively low speed.

After performing durability tests and determining basic material parameters, the RSA-501 aluminium alloy sample was subjected to twist extrusion processing in order to introduce structural changes and modify its durability parameters. Two RSA-501 aluminium alloy samples are pressed through the angular channel of the matrix, with only the first of the samples fully passing through the twisting area. The samples are pressed using a purpose-made cylinder rod, the mandrel of which enters the angular channel.

The SPD TE pressing test was performed using the same device that had earlier been used to tensile test. The device can be seen in Fig. 3.
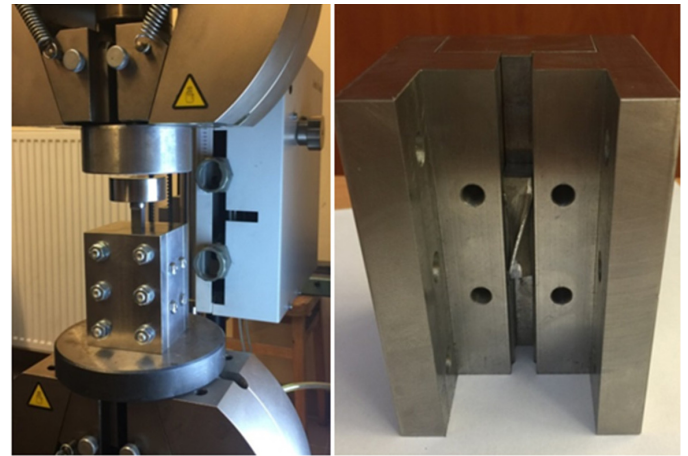

Fig. 3. Left – Instron 35 universal tensile test machine with Zwick-Roell measuring system, right – part of the matrix with visible of the channel to the TE test
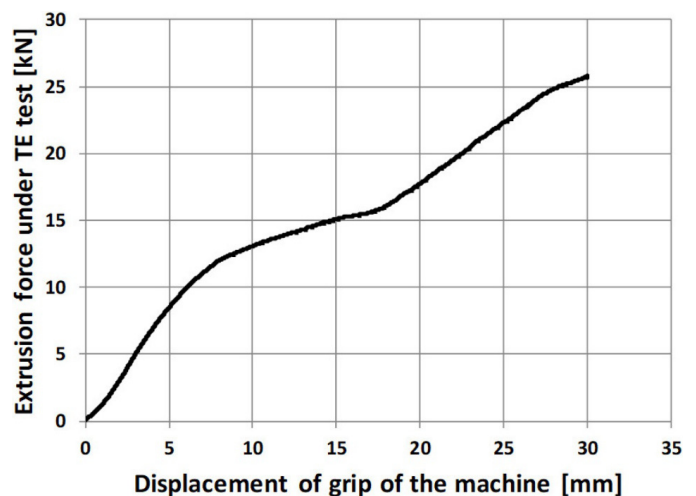

Fig. 4. Relationship between sample pressing force and the movement of the cylinder rod at the specified tensioning speed

The sample was pressed through the matrix at a constant speed and variable standard force. The highest force was gener-

ated when the cylinder rod was displaced by 30 mm in relation to its starting position (Fig. 4). The graph clearly shows the gradual increase of force until it reaches the local maximum (approx. 12 kN) and a further increase of force (after exceeding 15 kN).

Fig. 5 is a compiled graph that presents the relations between displacement of the front of the grip of the extruding test machine and the force which is corresponding this displacement. As seen on the graph, when the cylinder rod is displaced by 26 to 29 mm relative to the initial position, a slight drop in the force occurs – this is where the face of the sample reaches the exit from the angular channel (i.e. will shortly leave the angular channel area). After the relative displacement exceeds 30 mm, the face of the sample exits the angular channel and concludes the twisting process.

When the cylinder displacement exceeds 35 mm, the second sample enters the angular channel and is subjected to twisting.
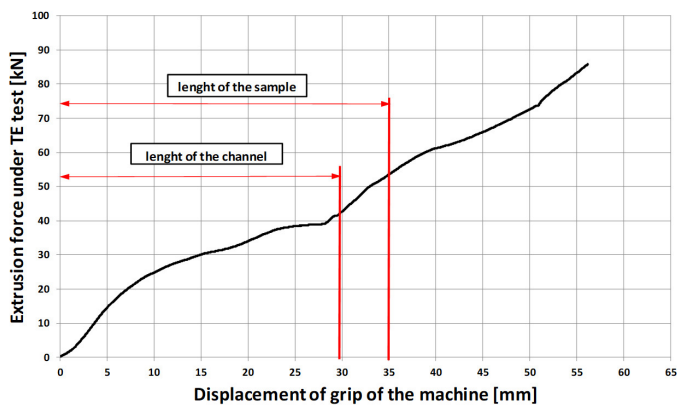

Fig. 5. Graph depicting the sample pressed through the matrix

Fig. 6 depicts photographs of samples subjected to twist extrusion processing. The bottom sample is the one that was the first to enter the angular channel and was fully twisted at a 90° angle. The top sample was used only for the purposes of aiding in performing the test by fully pushing the first sample through the angular channel.

Fig. 6a shows a plastically deformed samples edge. The device for the TE test is made up of four parts, connected with screws. The die was made on a numerically controlled machine
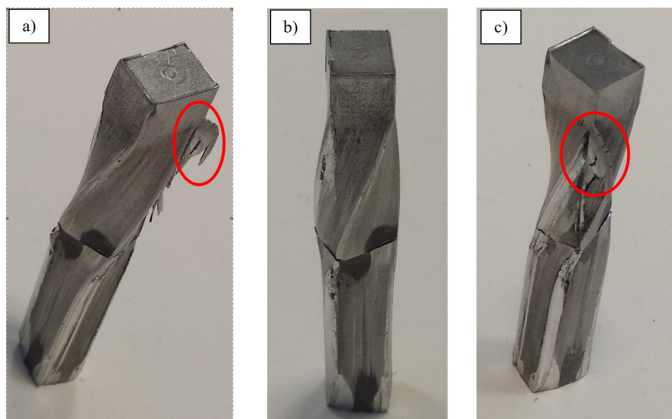
tool, and then the handle was thermo-chemical treated with sulfonation to raise the mechanical properties of the TE test tool. It is extremely difficult to explain why the situation shown in Fig. 6a and 6c occurred: the plastic flow and pressing part of the sample edge into the gap between the tool components, because after the test one of the parts of the TE holder was permanently deformed in small area/range but disqualifying handle as a tool for further research. Perhaps heat treatment is the reason, which deformed the tool and the deformation was not registered or the screws loosened during the TE test.

It can clearly be seen (Fig. 7) that the first sample (on the right) was fully twisted and passed through the angular channel, while the second sample (on the left) only partially entered the angular channel (part of the sample was not twisted). To remove the second sample, the matrix had to be taken apart.
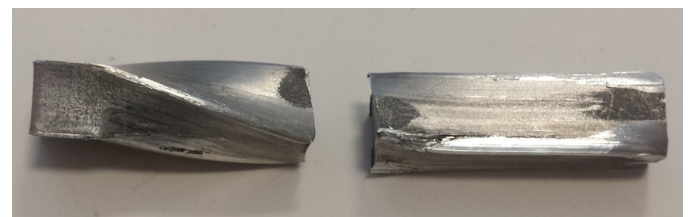

Fig. 7. Samples used in twist extrusion processing

3. Definition of the numerical model

Samples made of RSA-501 aluminium alloy, with a prismatic cross-section and dimensions of 8×10×35 mm, were used to simulate the twist extrusion pressing test (the samples used in durability testing were made of the same material).

The matrix model used in the simulation was prepared based on the actual matrix (Fig. 8) used to perform the twist extrusion process.
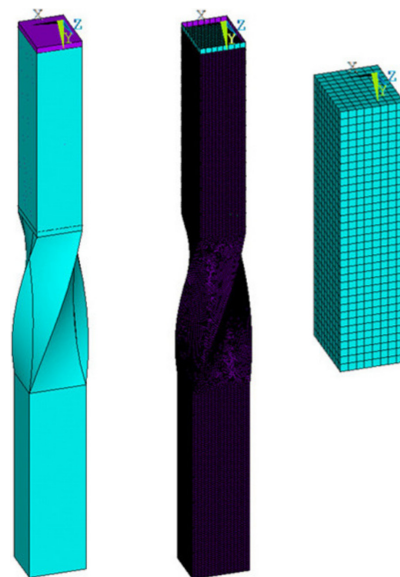

Fig. 8. The matrix for the Twist Extrusion treatment and geometric model for numerical analysis

Fig. 6. Samples pressed through the matrix

1388

Numerical modelling for the twist extrusion process was performer using the ANSYS® finite element suite. The numerical analysis was performed in order to analyse the distribution of stresses in the sample passing through the matrix. For the purposes of the numerical analysis it was assumed that the angular channel of the matrix is rigid and non-deformable, which allowed us to analyse the distribution of stresses without having to account for the phenomena occurring within the matrix. The channel was defined as stiff and undeformable. Testing concerned the behaviour of the sample entering and passing through the twisting area, up until the moment where the face of the sample was twisted at a 90° angle (i.e. only the face of the sample fully passed through the twisting area, and not the entire sample). The sample was discretized by second order brick element with twenty nodes, with three degree of freedom on each node. FEM model of material was made on base of the tensile test of the aluminium alloy which was used under test. The grid size has been selected to provide an acceptable solution time with a relatively small stress change in the model. By reducing the size of the grid twice, the time of solving one step increased several times, while the change in plastic strain did not exceed 5%.

The size of the task was set at slightly over 300,000 degrees of freedom. On base of the tensile test curve presented on Fig. 1, σ_{true}-ε_{ln} curve was calculated and this curve was applied to the FEM model of the sample. Using this curve is very important because the strain during the twisted extrusion test is very higher than yield stress and as we can see on Fig. 6 there are places where we can see destruction of the aluminium alloy also. Area of the destruction have an influence for the experimental curve presented on the Fig. 18. The influence of the destructions of the part of the aluminium alloy for the experimental curve of the twisted extrusion will explained in the part devoted conclusions.

The sample was loaded with a displacement equal to the length of the angular channel. The dynamic friction parameter was set at 0.08, while static friction was set at 0.05. Calculations accounted for geometric and material nonlinearities. 100 calculation steps were set and the automatic integral step densification function was activated.

4. Results of MES testing

Figures 9-11 depict the distribution of regular and shear stresses on the surface of the sample during the twist extrusion process. Analysis was performed in respect of a sample entering and moving through the twisting area, up until the full twisting of the base of the sample (meaning that only the base of the sample is twisted at a 90° angle, and not the entire sample).

As the sample passes through the twisting area, stresses of approx. 314 MPa appear an almost the entire surface of the sample, which constitutes a value only 5.5% higher than the value measured during the experiment (however, it must be noted that only the mean value of stresses was recorded during experimental tests, while the numerical analysis made it possible to observe the distribution of stresses, and stresses of 341 MPa
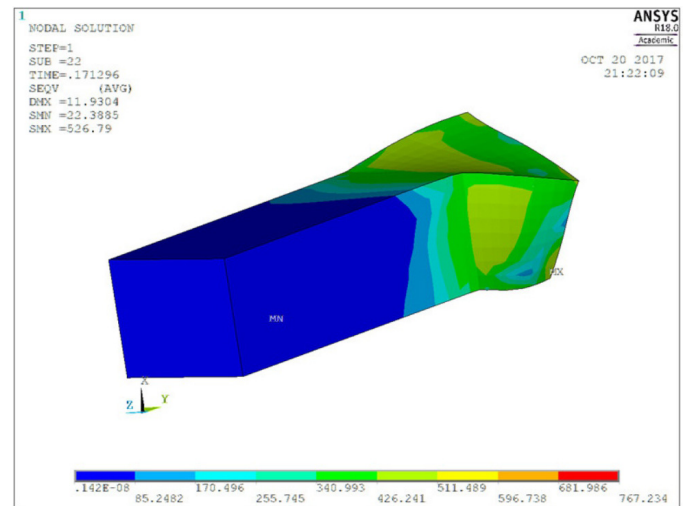
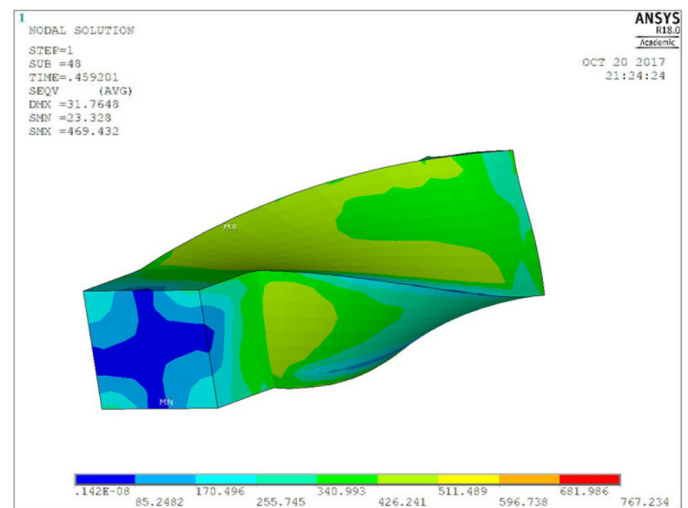
Fig. 9. Sample entering the twisting area

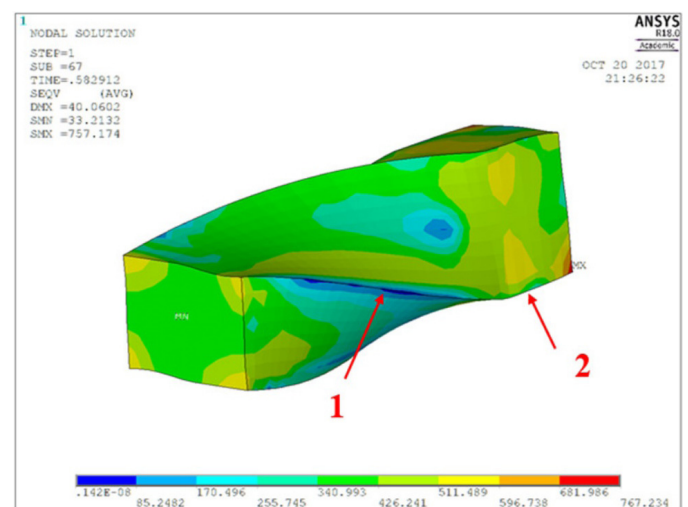Fig. 10. Sample inside the twisting area

Fig. 11. Sample exiting the twisting area

are the dominant stresses on the surface of the sample, and not the mean value of stresses).

As seen in Fig. 11, the highest stresses (approx. 597 MPa) appear on the tips of the face of the sample as it exits the twisting area (i.e. is twisted at a 90° angle). The above is caused by secondary hardening – the exit of the sample from the twisting area.

An interesting fact is that stresses with a value of approx. 170 MPa start to appear even before the sample enters the twisting area, as seen in Figs. 9-11.

It's also worth noting that when the sample passes through the twisting area, the lowest stress values are present on the side edges (marked with arrow number 1 in Fig. 11), while the highest stress values are present on the side edges and base edges when the sample exits the twisting area (Fig. 11, arrow number 2).

Higher stress values on the edges of the sample are caused by the friction (deformation) of the material against the matrix surface.

Figs. 13-15 show the distribution of shear stresses at the entry into the twisting channel, during the passage through the channel and at the exit from the channel (i.e. the conclusion of the twist extrusion process). Fig. 12 is a schematic depiction of the analysed plane.
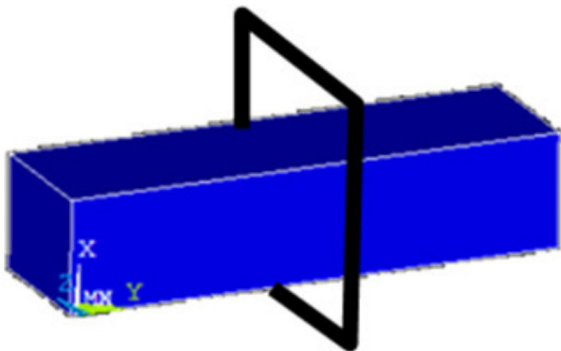

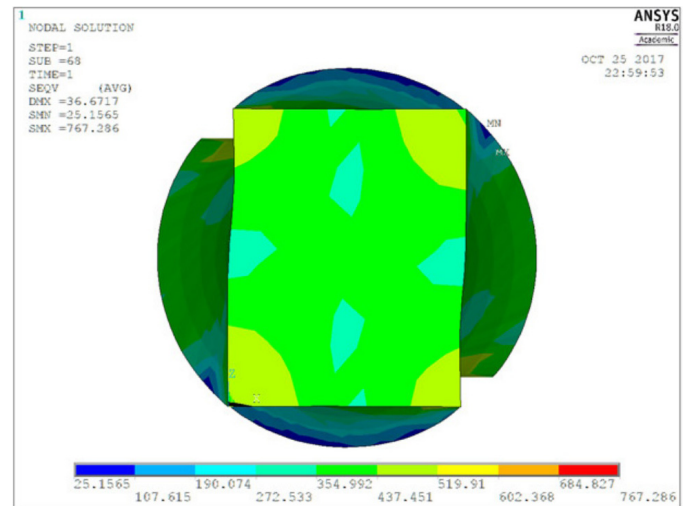Fig. 12. Schematic presentation of the analysed surface

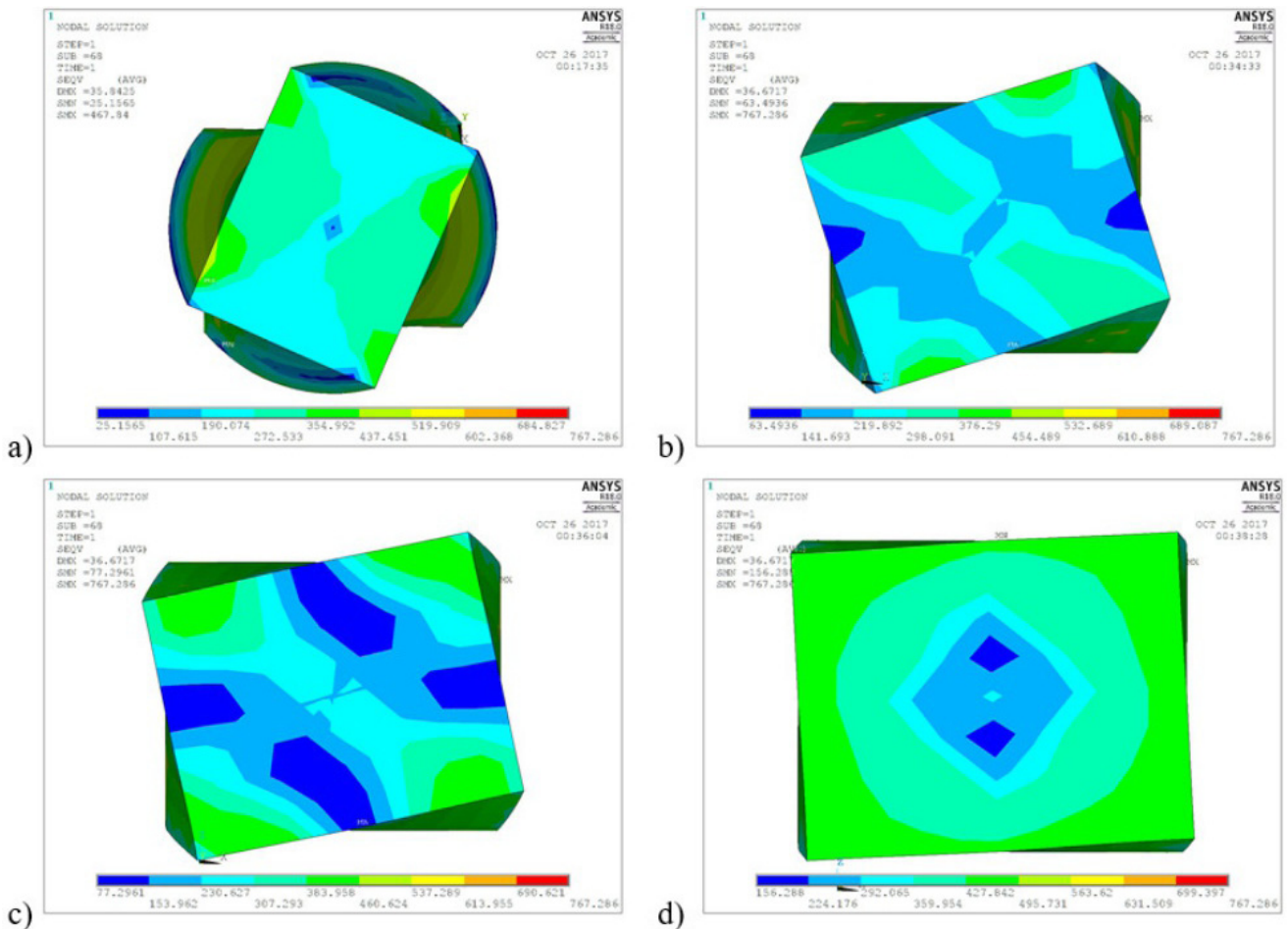Fig. 13. Distribution of stresses on the sample cross-section at the entry into the twisting area

a)

b)

c)

d)

Fig. 14. Distribution of stresses on the sample cross-section during the passage through the angular channel
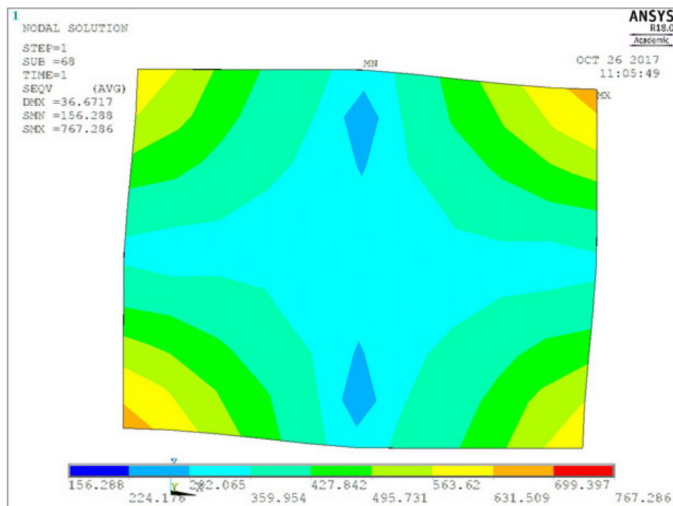
1390

Fig. 15. Distribution of stresses on the face of the sample at the exit of the twisting area

As seen in figs. 13-15, the distribution of stresses in the sample cross-section and the values of stresses varied and depended on the stage of the twisting process that the surface was subjected to at a given moment.

The lowest stress values were observed in the central area of the cross-section (i.e. in the midsection of the twisted sample, along the twisting plane), before and just after twisting the sample at a 45° angle, and fluctuate within the range of 28.5-63.5 MPa (lower values were observed before the sample was twisted at a 45° angle).

Fig. 15 depicts the phenomenon that could be seen in figs 9-11, namely that the highest stress values can be observed on the tips of side edges, at the entry into the angular channel. Fig. 16 depicts the plane of the 'bisection' that was made to illustrate the distribution of stresses inside the sample. Fig. 17 depict the distribution of stresses inside the sample (on the cross-sectional plane, parallel to the side wall of the sample and passing through its centre).
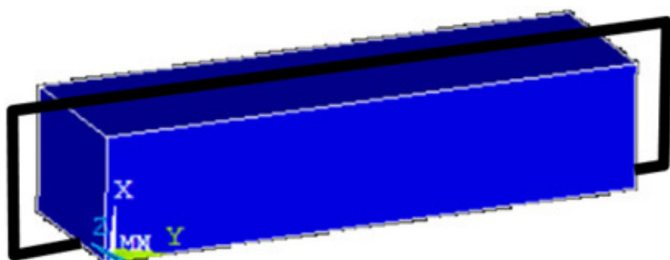

Fig. 16. Schematic presentation of the analysed surface

Fig. 17 clearly indicate that the highest stress values (approx. 420 MPa) appear on the surface 'entering' the angular channel.

By analysing the distribution of stresses on the sample surface, it becomes evident that the highest stress values appear on the outer edges that are subject to the most potent deformation processes, while the lowest stress values appeal along the

axis passing through the centre of the sample, parallel to the direction in which the sample is pressed, as this area is subject to the weakest twisting forces (Fig. 17c-d area marked in black).

Analysis of stresses on the surface of the cross-section and longitudinal section of the sample, as well as on its external surface (Figs. 9-11) indicates that the highest stress values appear on the tips of the face of the sample (tips of the cross-section) as the sample exits the twisting area, and may reach up to approx. 630 MPa. As stated above, this phenomenon is caused by secondary hardening. Lowest stress values appear in the central part of the section (the closer to the centre, the lower the stresses, as the central section of the sample is subject to the weakest twisting force).

Fig. 18 shows comparison of the results obtained from the TE tests with the results obtained from calculations using the FEM method. Experimental results are marked in blue, while the red line illustrates the results of numerical analysis. In the initial phase up to 10 kN, correspondence between experimental tests and the results of numerical calculations is observed. After exceeding the load of 10 kN, the force in the experiment continues to increase while in the FEM experiment it stabilizes and to displacement about 30 mm it has a constant value. It should be remembered that the FEM numerical solution is ideal, i.e. the channel has perfect dimensions, constant roughness and the most important that is uniform. For the real experiment, the channel was made in the form of four separate elements bolted with screws due to the high degree of complexity associated with its performance. As mentioned earlier, in order to improve the mechanical properties of the channel, all the elements were sulphonated, which significantly increases the mechanical properties and reduces the coefficient of friction. Deformations or inaccuracies in the channel design caused that one of the edges of the squeezed sample was pressed into the gap between the quarters of the channel (Fig. 6a). This situation takes place from 4 mm displacement where the force increases significantly. Although the differences in strength between FEM and TE test are very significant, it is easy to see similarities in the graph. In both cases an increase in force can be observed at the moment when the sample exits the channel (about 30-35 mm) and moves in its last part. In numerical analysis, additionally we observe at this stage of processing a significant drop in force which results only from the movement of the sample through the untwisted TE matrix channel.

5. Conclusions

The research performed during the experiment made it possible to:

1. Tensile strength of RSA-501 is not depending of velocity of load during experimental tests.
2. The use of numerical methods in the TE processes that use significant deformation accumulation is much more cost effective in comparison to experimental research and allows for analysing both the distribution of stresses and strains,
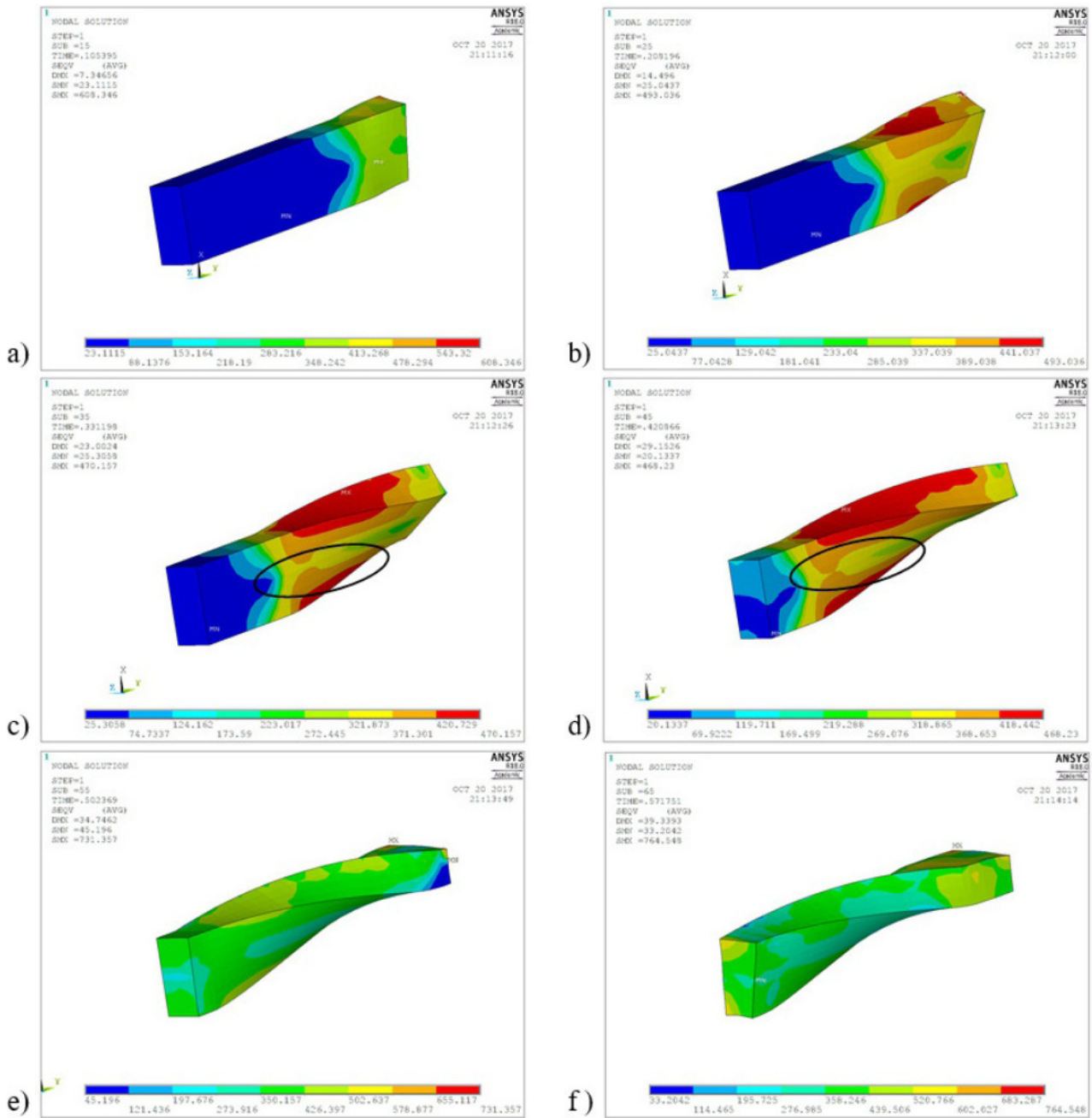
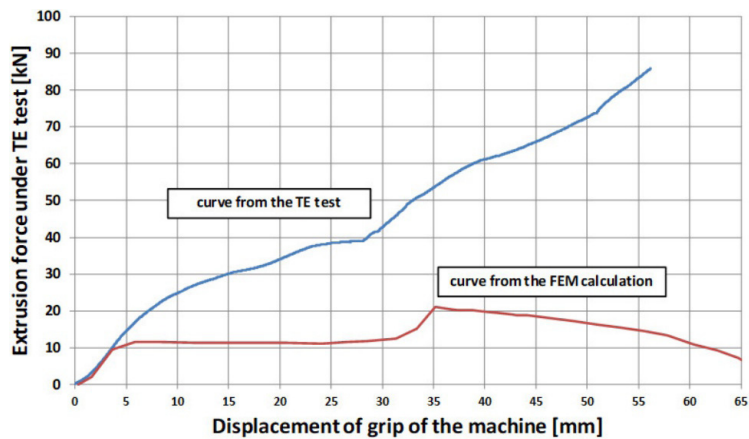Fig. 17. Distribution of stresses in the cross-sectional plane of the sample

Fig. 18. Graph compiled using data from the TE test and FEM test

1392

3. Observe the distribution of residual stresses with a value of approx. 340 MPa, generated during the TE process

4. Determine the actual parameters of force required to displace the sample during the process, confirming the significant effect of friction on the values of pressing forces. Numerical analysis confirms that the 20 kN of load is necessary to deform the sample during the begging and end of matrix channel.

5. The next stage of research requires the design and re-designing of the duct and its construction so that in the next test no pressed of the aluminum alloy in the gap between the components of the TE process matrix is noticed.

REFERENCES

[1] A. Zaki, U. Anwar, Corr. Sci. **43**, 1227-1243 (2001).

[2] S. Costa, H. Puga, J. Barbosa, A.M.P. Pinto, Mat. Sci. and Design. **42**, 347-352 (2012).

[3] M.J. Starink, Mat. Sci. Eng. A-Struct **705**, 42-45 (2017).

[4] Y.B. Xu, W.L. Zhong, Y.J. Chen, L.T. Shen, Q. Liu, Y.L. Bai, M.A. Meyers, Mat. Sci. Eng. A-Struct. **299**, 287-295 (2001).

[5] K. Rodak, J. Pawlicki, J. Mater. Sci. Technol. **27**, 1083-1088 (2011).

[6] H. Jia, K. Marthinsen, Y. Li, Trans. Nonferrous Met. Soc. China **27**, 971-976 (2017).

[7] M.S. Shadabroo, A.R. Eivani, H.R. Jafarian, S.F. Razavi, J. Zhou, Mater. Charact **112**, 160-168 (2016).

[8] H. Jia, R. Bjørge, K. Marthinsen, R.H. Mathiesen, Y. Li, Mat. Sci. Eng. A-Struct. **703**, 304-313 (2017).

[9] S.M. Baek, A.V. Polyakov, J.H. Moon, I.P. Semenova, R.Z. Valiev, H.S. Kim, Mat. Sci. Eng. A-Struct. A **707**, 337-343 (2017).

[10] T. Krajňák, P. Minárik, J. Stráský, K. Máthis, M. Janeček, Mat. Sci. Eng. A-Struct., Available online 24 October 2017, https://doi.org/10.1016/j.msea.2017.10.076.

[11] Z. Li, B. Wang, S. Zhao, R.Z. Valiev, K.S. Vecchio, M.A. Meyers, Acta Mater. **125**, 210-218 (2017).

[12] M.A. Meyers, A. Mishra, D.J. Benson, Prog. Mater. Sci. **51**, 427-556 (2006).

[13] R. Azushima, A. Kopp, D. Korhonen, Y. Yang, F. Micari, G.D. Lahoti, P. Groche, J. Yanagimoto, N. Tsujii, A. Rosochowskij, A. Yanagidaa, CIRP Ann-Manuf. Techn. **57**, 716-735 (2008).

[14] Ł. Kaczmarek, P. Kula, J. Sawicki, S. Armand, T. Castro, P. Kruszyński, A. Rochel, Arch. Metall. Mater. **54** (4), 1199-1205 (2009).

[15] M. Ensafi, G. Faraji, , H. Abdolvand, Mater. Lett. **197**, 12-16 (2017).

[16] C. Granato de Faria, N. Geraldo Silva Almeida, M.T.P. Aguilar, P.R. Cetlin, Mater. Lett. **174**, 153-156 (2016).

[17] M. Jahedi, M. Hossein Paydar, Mat. Sci. Eng. A-Struct. **528**, 8742-8749 (2011).

[18] B. Cherukuri, T.S. Nedkova, R. Srinivasan, Mat. Sci. Eng. A-Struct. **410-411**, 394-397 (2005).

[19] A. Staszczyk, J. Sawicki, Adv. Sci. Technol. Res. J. **11** (2), 51-57 (2017).

[20] V. Varyukhin, Y. Beygelzimer, S. Synkov, D. Orlov, Mater. Sci. Forum **503-504**, 335-340 (2006).

[21] M. Seyed Salehi, N. Anjabin, H.S. Kim, Met. Mater. Int. **20**, 825-834 (2014).

[22] S. Rusz, L. Cizek, M. Salajka, S. Tylsar, J. Kedron, V. Michenka, T. Donic, E. Hadasik, M. Klos, Arch. Metall. Mater. **59**, 359-364 (2014).